atmosphere

MDPI

Article

Investigating the Synergy between CO_2 and $PM_{2.5}$ Emissions Reduction: A Case Study of China's 329 Cities

Shangjiu Wang [1,2], Shaohua Zhang [1,*] and Liang Cheng [3]

[1] School of Economics and Statistics, Guangzhou University, Guangzhou 510006, China; wsj@sgu.edu.cn
[2] School of Mathematics and Statistics, Shaoguan University, Shaoguan 512005, China
[3] School of Political Science and Law, Shaoguan University, Shaoguan 512005, China; liang.cheng@sgu.edu.cn
* Correspondence: zsh104601@gzhu.edu.cn

Abstract: The synergetic reduction of CO_2 and $PM_{2.5}$ emissions has received much attention in China in recent years. A comprehensive evaluation of the synergy between CO_2 emission reduction (CER) and $PM_{2.5}$ emission reduction (PER) would provide valuable information for developing synergetic control policies. Thus, we constructed a comprehensive CO_2-$PM_{2.5}$-emission-reduction index system and evaluated the synergy between CER and PER, using the coupling coordination degree (CCD) and relative development degree (RDD) model in China's 329 cities from 2003 to 2017. The spatiotemporal characteristics of the CCD were analyzed on the national, regional, and urban scales. Furthermore, we used the spatial autocorrelation analysis, kernel density estimation, and Dagum Gini coefficient to investigate the spatial autocorrelation, evolutionary characteristics, and regional differences of the CCD. The results indicate that (1) the synergy between CO_2 and $PM_{2.5}$ emissions' reductions showed an upward trend, and the lowest CCD values occurred in NW and Shanghai on the regional and urban scales, respectively; (2) the CCD showed obvious spatial clustering characteristics, with 75% of the cities located in the "High–High" or "Low–Low" clustering zones in the Moran scatter plots in 2017; (3) the polarization of CCD in SC, MYR, and SW showed intensified trends; (4) and the hypervariable density was the largest contributor to the overall difference in the CCD. Our findings suggest that more attention should be paid to the top-level design of the policies, technological innovation, and cross-regional or intercity cooperation.

Keywords: CO_2 emission reduction; $PM_{2.5}$ emission reduction; synergy; coupling coordination degree model; Dagum Gini coefficient

Citation: Wang, S.; Zhang, S.; Cheng, L. Investigating the Synergy between CO_2 and $PM_{2.5}$ Emissions Reduction: A Case Study of China's 329 Cities. *Atmosphere* **2023**, *14*, 1338. https://doi.org/10.3390/atmos14091338

Academic Editors: Chong Wei, Chong Shi, Nan Li and Xingjun Xie

Received: 31 July 2023
Revised: 15 August 2023
Accepted: 21 August 2023
Published: 24 August 2023

1. Introduction

During the past decades, China has been undergoing rapid industrialization and urbanization. As a result, energy consumption has increased dramatically in China, increasing from 571 million tons of standard coal in 1978 to 4.98 billion tons of standard coal in 2020. Huge energy consumption has produced large quantities of greenhouse gases and atmospheric pollutants [1–4], threatening the ecological environment and public health [5,6]. In 2022, China issued the "Implementation Plan for Synergistic Reduction in Pollution and Carbon Emission". It proposed that to ensure the green development of the economy and society, coordinating the work on controlling CO_2 emissions and atmosphere pollution is essential [7]. China is facing the new challenge of synergizing carbon and pollution reduction. In this context, to provide more information for formulating emission-reduction measures, assessing the synergy level between CO_2 and $PM_{2.5}$ emissions' reduction is of great importance.

CO_2 emissions lead to some environmental problems. High levels of atmospheric CO_2 prevent heat from escaping the Earth, gradually raising the global average temperature and changing the Earth's climate. In addition, CO_2 dissolves in seawater, causing ocean acidification [8]. China is a large emitter of CO_2, contributing 30.7% of total global fossil

fuel emissions in 2020 [9,10]. To cut CO_2 emissions, China formulated the "Action Plan for carbon dioxide peaking by 2030" in 2021, focusing on improving non-fossil energy share and energy efficiency. Specifically, by 2030, the share of non-fossil energy consumption is expected to reach around 25%, and CO_2 emission intensity (i.e., CO_2 emissions/GDP) is expected to be reduced by more than 65% compared with 2005.

Atmosphere pollution, especially respirable fine particulate matter ($PM_{2.5}$), has been associated with various health problems, such as stroke, ischemic heart disease, lung cancer, etc., thereby increasing the risk of premature death [11–14]. In January 2013, China experienced large-scale and long-lasting haze pollution (dominated by $PM_{2.5}$) [15], which covered an area of more than 1.4 million square kilometers, affected approximately 800 million people, and lasted for almost one month [16–18]. In 2013, the annual average $PM_{2.5}$ concentration in nearly all key monitoring cities (96%) in China failed to meet the air-quality standard. Within this context, China has carried out many strict measures to reduce $PM_{2.5}$ emissions [19,20], significantly enhancing air quality. For all the cities at the prefecture level or above, the annual average $PM_{2.5}$ concentration was 36 $\mu g/m^3$ in 2019, decreasing by 28% compared to 2015; the days with good quality reached 82% in 2019, 0.8 percentage points higher than that of 2015. However, the situation for $PM_{2.5}$ pollution control remains grim, with heavy-pollution weather occurring frequently in the autumn and winter in some regions, such as the Fenwei Plain, and more than half of the country's cities still experiencing heavy-pollution weather.

The fossil-fuel-dominated energy structure determines a high degree of homology between CO_2 and $PM_{2.5}$ emissions in China [21], and this particular co-rooted property makes it possible to synergize CO_2 emission reduction (CER) and $PM_{2.5}$ emission reduction (PER) [22]. Previously, many studies have focused on the co-benefit of PER from CER. Some scholars examined the impact of CER policy on PER. They found that the policies primarily aimed at reducing CO_2 emissions, such as the low-carbon city pilot policy and emissions trading system pilot programs, played important roles in alleviating $PM_{2.5}$ pollution [23,24]. In addition to reducing $PM_{2.5}$ emissions, Chen and Wang also found that a long-term emission trading scheme policy could decrease $PM_{2.5}$-associated morbidity and mortality [25]. Some studies quantitatively assessed the impact of CO_2 emissions on $PM_{2.5}$ emissions. For instance, Dong et al. [26] used the log-mean division index (LMDI) method to investigate the drivers of $PM_{2.5}$ emission changes in China, finding that the synergistic effect of CER was the largest contributor to PER. Jia et al. [27] employed a similar method to decompose $PM_{2.5}$ emissions from coal consumption, proving CER's obvious role in PER. In addition, some studies have analyzed the co-benefit of CER from $PM_{2.5}$ pollution control policies and measures. For example, Shi et al. [28] examined the effect of clean-air actions on CER in China from 2013 to 2020. They found that the clean-air policy led to a considerable reduction in CO_2 emissions (2.43 Gt) over the period. Yang et al. [29] evaluated the synergistic effect of $PM_{2.5}$-pollution-abatement policies on CO_2 emissions in China's iron and steel industry. They found that those policies could simultaneously achieve CO_2-emission-reduction goals. Xing et al. [30] confirmed that the Blue Sky Defense Action Plan promoted the CO_2 emission abatement in Tangshan City in China.

The quantitative assessment of the synergy degree between CER and pollutant reduction has received increasing concern [5]. Yi et al. [21] first constructed composite indexes for CER and air-pollution control, respectively, and then calculated the synergy degree between the two composite indexes, using a synergy degree model in China's 30 provinces during 2005–2018. They found that Guangdong Province performed best in the synergy degree among all the provinces due to its optimal industrial structure. Using provincial data from 2011 to 2019, Tang et al. [31] first developed a composite air-pollutant index (i.e., pollutant emission equivalent). Then, they adopted the coupling coordination degree (CCD) model to evaluate the synergy between CO_2 emissions and the pollutant emission equivalent in China. Similarly, Nie et al. [32] employed the CCD model to assess the synergy between CER and pollution control in China's provinces. When classifying the synergy states, both Tang et al. [31] and Nie et al. [32] divided the CCD values into several groups in a subjective

manner. As for the synergy between CER and PER, based on the gridded data, Li et al. [33] characterized the changes in CO_2 emissions and $PM_{2.5}$ concentrations in China with the four-quadrant diagram from 2005 to 2015. They compared the differences in the changes in CO_2 emissions and $PM_{2.5}$ concentrations in China's three urban agglomerations, finding that the Pearl River Delta showed the best performance in the synergistic reduction.

Some deficiencies can be identified in the previous studies. Firstly, most studies assessed the synergy between CER and pollution reduction at the provincial level or above. However, the city is China's basic unit for synergistic emission reduction [34,35]. It concentrates many people, industrial activities, and transportation, releasing a large volume of pollutants and greenhouse gas [36,37]. Conducting the synergy evaluation on the urban scale in China is essential. In addition, though some scholars have investigated the synergy between CER and pollution reduction, the study on the synergy between CER and PER is insufficient. Secondly, in the existing research, the single variables, i.e., CO_2 emissions and $PM_{2.5}$ concentrations, were used to represent the level of CER and PER, respectively [5,38]. However, the emission intensity and growth rate of emissions are also critical for measuring reduction levels. It is necessary to construct comprehensive indicators for CER and PER, respectively. Moreover, because $PM_{2.5}$ concentrations are easily influenced by meteorological conditions and topography, using them to represent the PER level is imprecise. Thirdly, when classifying the synergy states based on the results of the CCD model, most studies adopted a subjective method to divide the CCD values into different levels, which may lead to an inaccurate division when the values are not uniformly distributed [39]. In addition, the relative development state between CER and pollution reduction was not taken into account in the existing studies. Whether CER lags behind pollution reduction or pollution reduction lags behind CER is unclear.

Therefore, using data from China's 329 cities from 2003 to 2017, this study revealed the synergy between CER and PER in China's 329 cities from 2003 to 2017. The specific objectives of this study were to (i) evaluate the synergy between CER and PER with the CCD model and relative development degree (RDD) model; (ii) characterize the spatiotemporal characteristics, spatial autocorrelation, and evolutionary characteristics of the synergy with a spatial autocorrelation analysis and kernel density estimation; and (iii) reveal the regional differences in the synergy with Dagum's Gini coefficient.

The contributions of the present study are as follows: (1) Selecting the city as the primary research unit, this study evaluated the synergy between CER and PER in China and further revealed the spatiotemporal characteristics, spatial autocorrelation, evolutionary trends, and regional differences of the synergy. This study can enrich the research on the synergy between CER and PER. (2) To more accurately characterize the CER and PER levels, the study constructed composite indexes for CER and PER, respectively, from three aspects, namely total emissions, emission intensity and growth rate of emissions. (3) This study evaluated the synergy between CER and PER by using the CCD model. The synergy levels were classified with an objective method, i.e., the quartile method. Moreover, the RDD model was used to explore the relative development state between CER and PER.

The rest of the paper is organized as follows: Section 2 presents the materials and methods. Section 3 presents the empirical results. Section 4 discusses the empirical findings. Finally, Section 5 presents the conclusions and policy implications of the paper.

2. Materials and Methods

A three-step approach was designed for the study (Figure 1). First, a comprehensive CO_2-$PM_{2.5}$-emission index system was developed, and the weights of the indicators were calculated using the entropy method. Combing the CCD model and RDD model, the synergy between CER and PER was assessed. Second, using the spatial autocorrelation analysis and kernel density estimation methods, the spatial and temporal characteristics, spatial autocorrelation, and evolutionary characteristics of the synergy were explored. Third, the intra-regional and inter-regional differences in the synergy were distinguished, and the sources of the overall difference were investigated using Dagum's Gini coefficient.

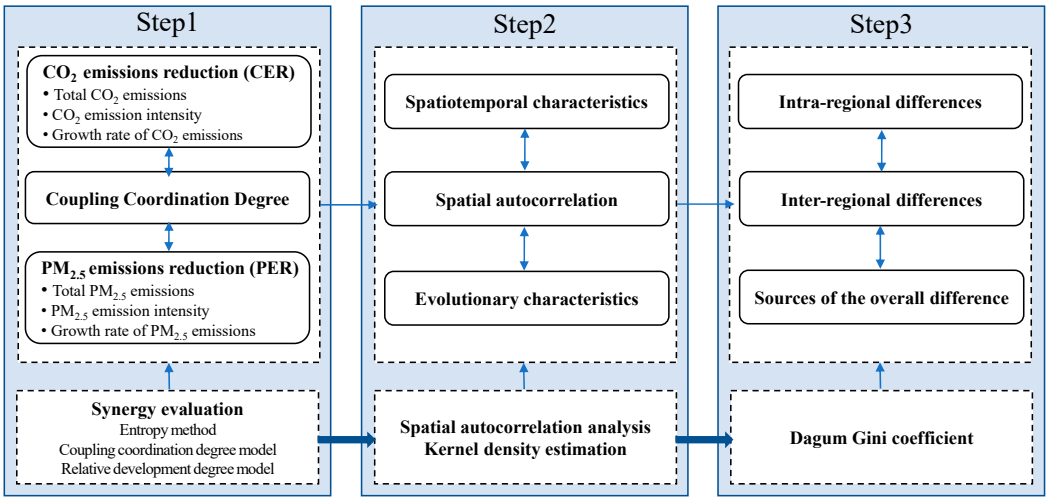

Figure 1. The framework of this study.

2.1. Study Area

This research was conducted on three spatial scales, namely the national, regional, and urban scales. On the urban scale, 329 prefecture-level-and-above cities were selected for the study (Figure 2). Cities in four provincial-level units (namely Tibet, Hong Kong, Macao, and Taiwan) and Sansha City were not covered because of the lack of data. On the regional scale, the cities were divided into eight regions, including Northeast (NE), North Coast (NC), East Coast (EC), South Coast (SC), Middle Yangtze River (MYeR), Middle Yellow River (MYR), Southwest (SW), and Northwest (NW) [40]. The full names of the cities in each region are shown in Appendix A Figure A1.

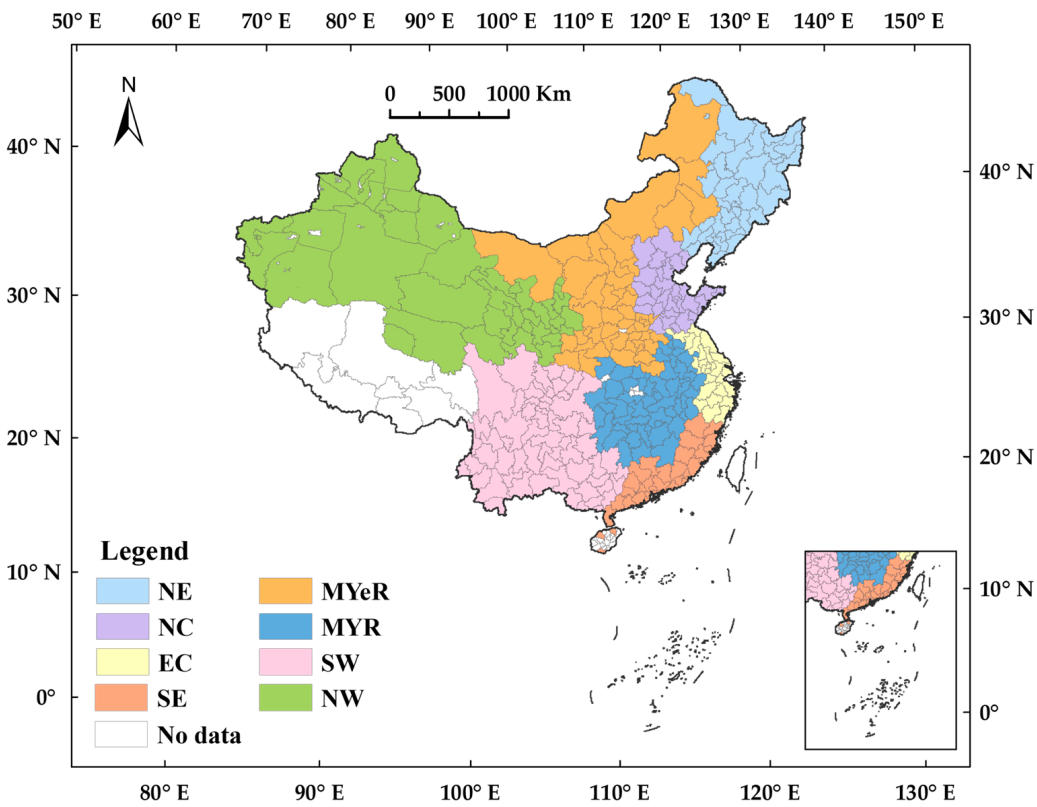

Figure 2. The locations of the 329 cities in China and the regional division.

2.2. The Evaluation Index System

Greenhouse gases and $PM_{2.5}$ often come from the same sources, which determines that there can be a strong synergistic effect between CO_2 and $PM_{2.5}$ emission reductions. Therefore, we constructed a comprehensive CO_2-$PM_{2.5}$-emission index system. The composite system consists of two subsystems, namely the CO_2 emission reduction (CER) subsystem and the $PM_{2.5}$ emission reduction (PER) subsystem. Then, following the principles of scientificity, independence, and credibility, we selected three indexes (i.e., total emissions, emission intensity, and growth rate of emissions) to measure the level of each subsystem (Table 1). As an absolute index, the total emissions directly reflect changes in CO_2 or $PM_{2.5}$ emissions. The emission intensity and growth rate of emissions are both relative indexes. The emission intensity is the amount of CO_2 or $PM_{2.5}$ emissions generated per unit of GDP, representing the abatement potential. The growth rate of emissions is another effective index for emission abatement evaluation, reflecting the trends in CO_2 or $PM_{2.5}$ emissions. Note that all the indexes are negative indicators for assessing CO_2 and $PM_{2.5}$ emission reductions. In other words, the lower the score, the better the subsystem. In addition, the Pearson correlation analysis was performed to examine the independence of the indicators within each subsystem. The correlations of any two indicators were low (Appendix A Figure A2).

Table 1. The comprehensive CO_2-$PM_{2.5}$-emission-reduction index system.

Subsystem	Indexes	Unit	Attributes	Weights
CO_2-emission-reduction subsystem	Total CO_2 emissions	10^6 ton	-	0.3333
	CO_2 emission intensity	Ton per 10^2 yuan	-	0.0228
	Growth rate of CO_2 emissions	%	-	0.6439
$PM_{2.5}$-emission-reduction subsystem	Total $PM_{2.5}$ emissions	Ton	-	0.2359
	$PM_{2.5}$ emission intensity	Ton per 10^8 yuan	-	0.0315
	Growth rate of $PM_{2.5}$ emissions	%	-	0.7326

2.3. Data Sources and Processing

The CO_2 emission data were obtained from China Emission Accounts and Datasets (https://www.ceads.net.cn/, accessed on 10 May 2023). Chen et al. [33] estimated the CO_2 emissions of 2375 counties in China, using provincial-level CO_2 emissions and nighttime light data. We then calculated the CO_2 emissions of each prefecture-level and above city by using the county-level CO_2 emission data. The $PM_{2.5}$ emission data with a spatial resolution of 0.1° were obtained from the annual $PM_{2.5}$ emission grid maps [41], which were provided by the Emissions Database for Global Atmospheric Research (https://edgar.jrc.ec.europa.eu/, accessed on 12 May 2023). The GDP data were collected from the China City Statistical Yearbook (https://data.cnki.net/yearBook/single?id=N2022040095, accessed on 15 May 2023). GDP was converted to constant 2000 prices by using the GDP deflator to remove the effect of price changes.

Since the indexes of the composite system vary in units and magnitude, the raw data were standardized using the following formula [42]:

$$z_{ijt} = \frac{x_{ijt} - \min(x_j)}{\max(x_j) - \min(x_j)}, \tag{1}$$

where x_{ijt} and z_{ijt} denote the original and standardized values of the jth indicator for city i in year t, respectively; and $\max(x_j)$ and $\min(x_j)$ indicate the maximum and minimum values. The minimum value for each indicator is 0 after standardization. Then, to facilitate the subsequent calculation of information entropy, all the 0 values were substituted with 0.0001 [43].

2.4. Calculation of the Subsystem Scores

2.4.1. Entropy Method

We used the entropy method to assign weights to the indexes. This method determines the weights of indexes according to the variations in the indexes, avoiding the interference of subjective factors [44]. The greater the variance in the values of one index, the more information the index can provide. Then, it should be assigned a higher weight. The details are as follows:

Step 1: Calculate the proportion of the value of index j of the evaluation object i in the year t to the sum of the values of the index j:

$$p_{ijt} = \frac{z_{ijt}}{\sum_{i=1}^{m}\sum_{t=1}^{h} z_{ijt}}, \tag{2}$$

Step 2: Calculate the information entropy, E_j, of index j:

$$E_j = -\frac{1}{\ln(h \times m)}\sum_{i=1}^{n}\sum_{t=1}^{h} p_{ijt}\ln p_{ijt}, \tag{3}$$

Step 3: Calculate the weight, w_j, of index j:

$$w_j = \frac{1 - E_j}{\sum_{j=1}^{n}\left(1 - E_j\right)}. \tag{4}$$

Using Equations (2)–(4), we obtained the weights of all the indicators (Table 1).

2.4.2. Comprehensive Evaluation Function

After determining the weights of indexes, we used the comprehensive evaluation function to calculate the scores of two subsystems.

$$CI_{it} = \sum_{j=1}^{n} w_j \times z_{ijt}, \tag{5}$$

$$PI_{it} = \sum_{j=1}^{n} w_j \times z_{ijt}, \tag{6}$$

where CI_{it} and PI_{it} denote the scores of CO_2-emission- and $PM_{2.5}$-emission-reduction subsystems, respectively; $CI_{it} \in [0, 1]$; and $PI_{it} \in [0, 1]$. A higher value of $CI_{it}(PI_{it})$ indicates the more excellent quality of the CO_2 ($PM_{2.5}$)-emission-reduction subsystem.

2.5. Evaluation of the Synergy between CER and PER

2.5.1. Coupling Coordination Degree Model

Two critical indicators in the coupling coordination degree (CCD) model are the coupling degree and CCD. The coupling degree describes the dependency, while the CCD reflects the level of coordination between the systems [45]. In order to reveal the synergy level between CER and PER, we developed a CCD model as follows:

$$C_{it} = 2\sqrt{CI_{it} \times PI_{it}}/(CI_{it} + PI_{it}), \tag{7}$$

$$D_{it} = \sqrt{C_{it} \times (\alpha PI_{it} + \beta PI_{it})}, \tag{8}$$

where C_{it} denotes the coupling degree, D_{it} indicates the CCD, and α and β are coefficients of the two subsystems. Since both subsystems contribute equally to the system, we took $\alpha = \beta = 0.5$. $C_{it} \in [0, 1]$; $D_{it} \in [0, 1]$. A higher C_{it} value indicates a stronger interaction

between CER and PER, and a higher D_{it} value indicates a higher coupling coordination level between the two subsystems. After calculating the CCD, we used the quartile method to divide the CCD values into four levels: low, medium, high, and extremely high. The quartile method takes three values at 25%, 50%, and 75% of the data as clinical values, ensuring a more objective classification [46].

2.5.2. Relative Development Degree Model

The relative development degree (RDD) model was used to assess the relative development status between CER and PER. The RDD is defined as follows [24]:

$$k_{it} = \frac{CI_{it}}{PI_{it}}, \tag{9}$$

where k_{it} denotes the RDD of CER and PER of evaluation object i in year t. When $0 < k_{it} \leq 0.9$, CER lags behind PER. When $0.9 < k_{it} \leq 1.1$, this indicates a state of synchronous development of CER and PER; when $k_{it} > 1.1$, PER lags behind CER.

2.6. Spatial Autocorrelation Analysis

To determine whether the spatial distribution of the synergy level is clustered, dispersed, or random, we used the Global Moran's I to explore the global spatial autocorrelation of the CCD. The formula is as follows [32]:

$$I = \frac{\sum_{i=1}^{n}\sum_{j=1}^{n} w_{ij}(x_i - \overline{x})(x_j - \overline{x})}{S^2 \sum_{i=1}^{n}\sum_{j=1}^{n} w_{ij}}, \tag{10}$$

where $\overline{x} = \sum_{i=1}^{n} x_i \Big/ n$; $S^2 = \sum_{i=1}^{n} (x_i - \overline{x}) \Big/ n$; n is the number of the space units; x_i and x_j are the attribute values of the space units i and j, respectively; and w_{ij} is the spatial weight matrix. $I \in [-1, 1]$. The spatial autocorrelation among attribute values is positive when $I > 0$ and negative when $I < 0$.

The Moran scatter plot can be used to visualize the Global Moran's I. The first quadrant of the scatter plot indicates that both the central spatial unit and its neighbors have high attribute values, known as "High–High cluster (HH)"; the second quadrant indicates that the central spatial unit has low attribute values, while its neighbors have high values, known as "Low–High cluster (LH)"; the third quadrant indicates that both the central spatial unit and its neighbors have low values, known as "Low–Low cluster (LL)"; and the fourth quadrant indicates that the central spatial unit has high attribute values, while its neighbors have low values, known as "High–Low cluster (HL)".

2.7. Kernel Density Estimation

The kernel density estimation (KDE) is a non-parametric approach [44] which can better depict the distribution shape of the continuous variable compared to the histogram. We used the KDE method to present the dynamic evolutionary process of the CCD. Let $\{x_1, \ldots, x_n\}$ be an n-dimensional random sample whose density function can be estimated as follows:

$$f(x) = \frac{1}{nh}\sum_{i=1}^{n} K\left(\frac{x_i - x}{h}\right), \tag{11}$$

where $K(\cdot)$ is the kernel function, and h is the bandwidth. The Gaussian kernel function was chosen for the estimation in this paper. The bandwidth value is of crucial practical importance for the kernel regression estimation. The accuracy decreases as the bandwidth increases. However, the density curve will be too spiky if the bandwidth is too small. We used the optimal bandwidth selection method to determine the bandwidth in this study.

2.8. Dagum Gini Coefficient

Traditional inequality indices, such as the Theil index and classical Gini coefficient, are based on normal distribution and homoscedasticity, requiring no overlap between grouped samples. Moreover, it is difficult to decompose the two indices into several economically significant sub-indices [47]. The Dagum Gini coefficient can effectively overcome the above defects [40]. We used the Dagum Gini coefficient (G) to investigate the regional differences in the CCDs. G can be calculated as follows:

$$G = \frac{\sum_{j=1}^{k}\sum_{h=1}^{k}\sum_{i=1}^{n_j}\sum_{r=1}^{n_h}\left|y_{ji} - y_{hr}\right|}{2n^2\overline{y}}, \tag{12}$$

where j and h denote different regions, respectively; i and r denote different cities, respectively; k and n are the numbers of regions and cities, respectively; $y_{ji}(y_{hr})$ is the CCD of city $i(r)$ in region $j(h)$; and $\overline{y}$ is the average value of the CCD of all the cities.

To perform the Dagum Gini coefficient decomposition, we first defined the Gini coefficient for the j-th region (G_{jj}) and the inter-regional Gini coefficient between the j-th and h-th regions (G_{jh}), as illustrated in Equations (13) and (14).

$$G_{jj} = \frac{\frac{1}{2\overline{y}_j}\sum_{i=1}^{n_j}\sum_{r=1}^{n_j}\left|y_{ji} - y_{jr}\right|}{n_j^2}, \tag{13}$$

$$G_{jh} = \sum_{i=1}^{n_j}\sum_{r=1}^{n_h}\frac{\left|y_{ji} - y_{hr}\right|}{n_j n_h\left(\overline{y}_j + \overline{y}_h\right)}, \tag{14}$$

where $n_j(n_h)$ is the number of cities in region $j(h)$, and $\overline{y}_j(\overline{y}_h)$ denotes the mean value of CCD for all cities in region $j(h)$.

Furthermore, G can be decomposed into three parts, namely the contributions of intra-regional differences (G_w), inter-regional differences (G_{nb}), and hypervariable density (G_t), i.e., $G = G_w + G_{nb} + G_t$. The detailed equations are as follows:

$$G_w = \sum_{j=1}^{k} G_{jj}p_j s_j, \tag{15}$$

$$G_{nb} = \sum_{j=2}^{k}\sum_{h=1}^{j-1} G_{jh}\left(p_j s_h + p_h s_j\right)D_{jh}, \tag{16}$$

$$G_t = \sum_{j=2}^{k}\sum_{h=1}^{j-1} G_{jh}\left(p_j s_h + p_h s_j\right)\left(1 - D_{jh}\right), \tag{17}$$

$$D_{jh} = \frac{d_{jh} - p_{jh}}{d_{jh} + p_{jh}}, \tag{18}$$

$$d_{jh} = \int_0^{\infty} dF_j(y)\int_0^{y}(y - x)dF_h(x), \tag{19}$$

$$p_{jh} = \int_0^{\infty} dF_h(y)\int_0^{y}(y - x)dF_j(x), \tag{20}$$

where $p_j = n_j/n$, $s_j = n_j\overline{y}_j/ny$, and $\sum p_j = \sum s_j = \sum_{j=1}^{k}\sum_{h=1}^{k} p_j s_h = 1$; D_{jh} indicates the relative impact of the CCD between regions j and h; d_{jh} is the mathematical expectation of the sum of all the sample values satisfying $y_{ji} - y_{hr} > 0$ in regions j and h; p_{jh} denotes the mathematical expectation of the sum of all the sample values satisfying $y_{hr} - y_{ji} > 0$; and $F_j(F_h)$ denotes the cumulative distribution function of the CCD of region $j(h)$.

3. Results

3.1. Spatiotemporal Characteristics of Coupling Coordination Level

According to Equations (1)–(8), we calculated the CCD of 329 Chinese cities from 2003 to 2017. Then, the CCD values were classified into four levels, using the quartile method: (1) low level ($0 \leq CCD < 0.8101$), (2) medium level ($0.8101 \leq CCD < 0.8316$), (3) high level ($0.8316 \leq CCD < 0.8526$), and (4) extremely high level ($0.8526 \leq CCD < 1$). To evaluate the overall synergy between the CER and PER of the whole country and eight regions, we also calculated the national average CCD and regional average CCD, respectively.

3.1.1. CCD on the National Scale

Figures 3a and 4a present the changing trends of the average CCD and the proportion of cities with different coupled coordination types in China, respectively. As shown in Figure 3a, the national CCD ranged from 0.7935 to 0.8710 during the whole period. Overall, the CCD presented an upward trend. It grew slowly from 2003 to 2011, at an average growth rate of 0.23%. Then, after 2012, the CCD entered a rapid growth stage, growing at an average growth rate of 0.90% and increasing by 5.58% within six years. The changes in the proportions of cities with different coupled coordination types also confirm a significant improvement in the overall coupling coordination level (Figure 4a). In 2003, the proportions of low-level, medium-level, high-level, and extremely high level coordinated cities were 79.33%, 19.15%, 1.52%, and 0, respectively. In 2017, the proportions of low- and medium-level coordinated cities decreased to 3.65% and 6.99%, respectively, while the proportions of high-level and extremely high level coordinated cities increased to 31.31% and 58.05%. The enhancement in the national CCD indicates that China has achieved remarkable results in the synergistic control of CO_2 and $PM_{2.5}$ emissions' reductions.

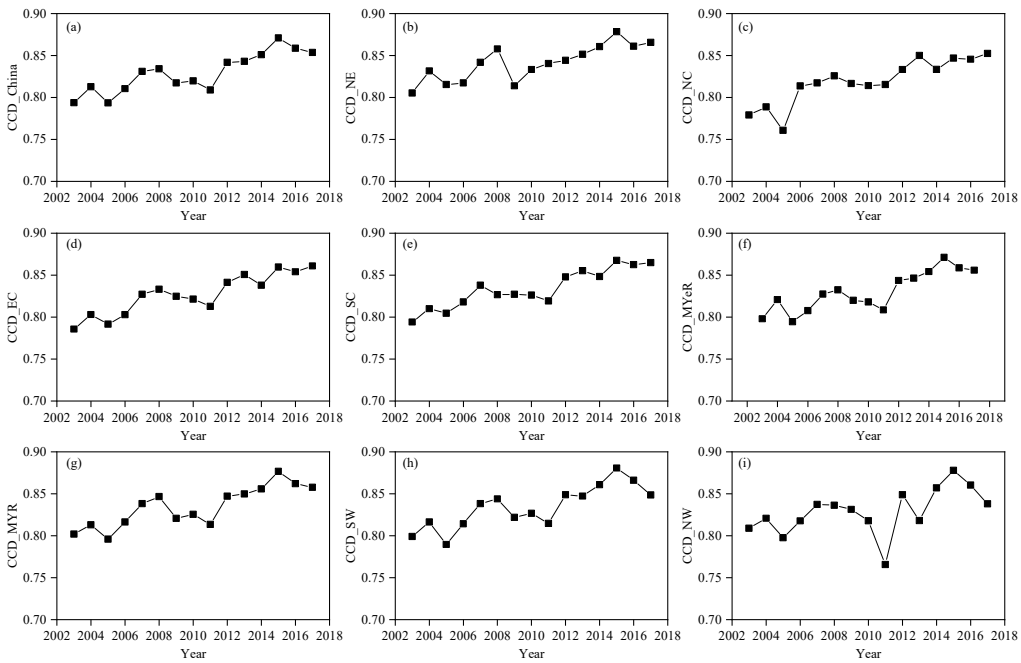

Figure 3. CCD of China and its eight regions from 2003 to 2017: (**a**) China; (**b**) NE; (**c**) NC; (**d**) EC; (**e**) SC; (**f**) MYeR; (**g**) MYR; (**h**) SW and (**i**) NW.

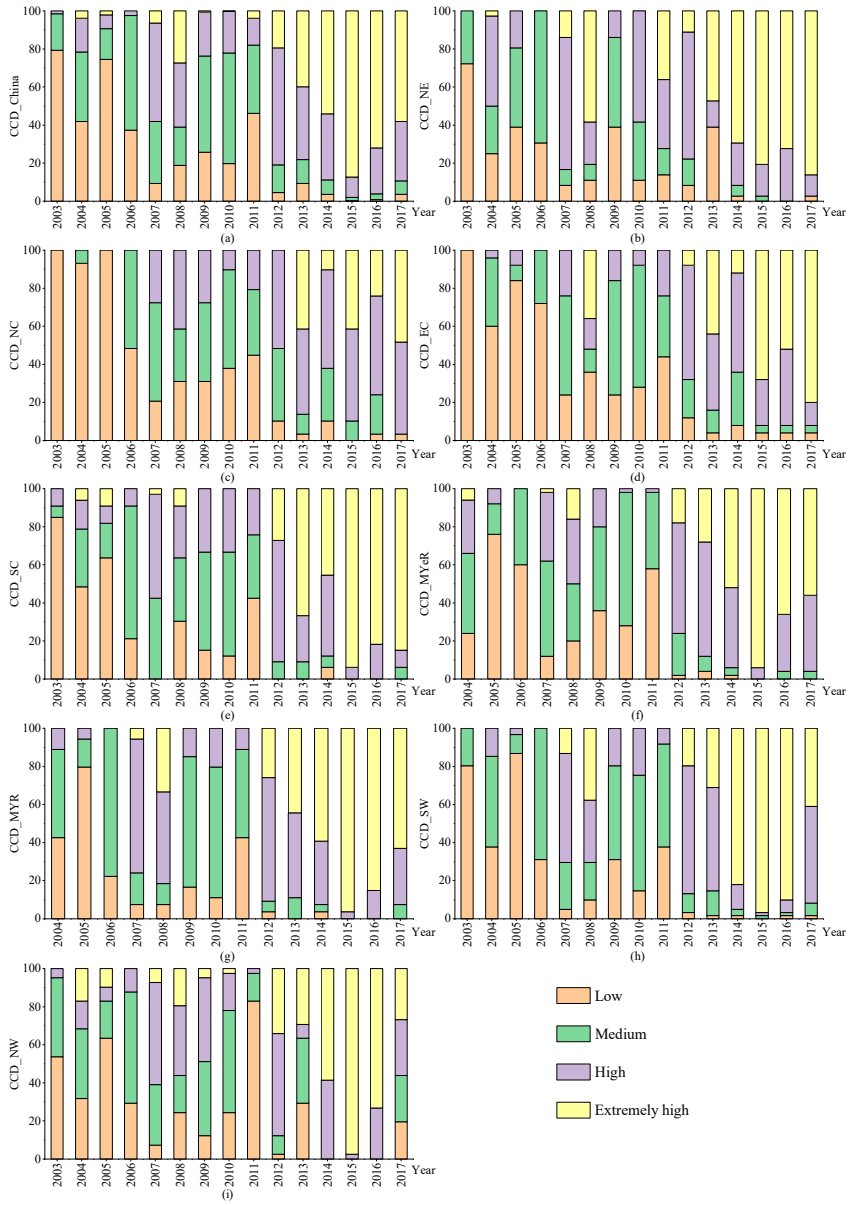

Figure 4. Proportions of cities with different coupled coordination types in China and its eight regions from 2003 to 2017: (**a**) China; (**b**) NE; (**c**) NC; (**d**) EC; (**e**) SC; (**f**) MYeR; (**g**) MYR; (**h**) SW and (**i**) NW.

3.1.2. CCD on the Regional Scale

Figure 3b–i show the changing trends of the average CCD in eight regions. In general, the CCD of all the regions presented increasing trends, but there were fluctuations during the study period, and fluctuation ranges varied for different regions. NE, SW, and NW showed large fluctuations in CCD, with values ranging from 0.7607 to 0.8785, from 0.7656 to 0.8808, and from 0.7656 to 0.8780, respectively. The fluctuation of CCD in SC was the smallest among the eight regions, and the CCD values were in the range from 0.7941 to 0.8677. The CCD of six regions (i.e., NE, SC, MYeR, MYR, SW, and NW) peaked in 2015 but dropped slightly afterwards. In 2017, the regional CCD followed the order of NE (0.8658) > SC (0.8651) > EC (0.8611) > MYR (0.8577) > MYeR (0.8559) > NC (0.8523) > SW (0.8485) > NW (0.8379).

Figure 4b–i display the changing trends of the proportions of the cities with different coupled coordination types in the eight regions. The proportions of extremely high level coordinated cities in all the regions, especially in NE, SC, and EC, showed clear upward trends. Specifically, no extremely high level coordinated cities were in NE, SC, and EC

in 2013. However, by 2017, the proportions of extremely high level coordinated cities accounted for 86.11%, 84.85%, and 80% in the three regions, respectively. In 2017, except for NW, the proportions of high-level and extremely high level coordinated cities in all the other regions were more than 90%; NW had 19.51% cities in low-level coordination and 24.39% in medium-level coordination.

3.1.3. CCD on the Urban Scale

Figure 5a,c,e illustrate the CCDs in 329 cities in 2003, 2010, and 2017. The CCD values in 329 cities were in the ranges of 0.6462–0.8427 in 2003, 0.6430–0.8537 in 2010, and 0.7382–0.9010 in 2017. During the whole period, the coupling coordination status of 329 cities shifted from low- and medium-level predominant coordination to high-level and extremely high level predominant coordination. In 2003, only five cities, namely Danzhou, Sanya, Haidong, Haikou, and Xining, were in high-level coordination, while all the other cities were in low- or medium-level coordination; Shanghai had the lowest CCD (0.6462). In 2010, Jiayuguan was in extremely high level coordination, and 72 cities were in high-level coordination; the lowest CCD was observed in Shanghai (0.6430), followed by Anshan (0.7325) and Chongqing (0.7524). In 2017, the number of extremely high level coordinated cities increased to 191, and the highest CCD was observed in Mudanjiang (0.9010); the CCD of Shanghai increased by 14.80%, but Shanghai was still in low-level coordination and had the lowest CCD among the cities.

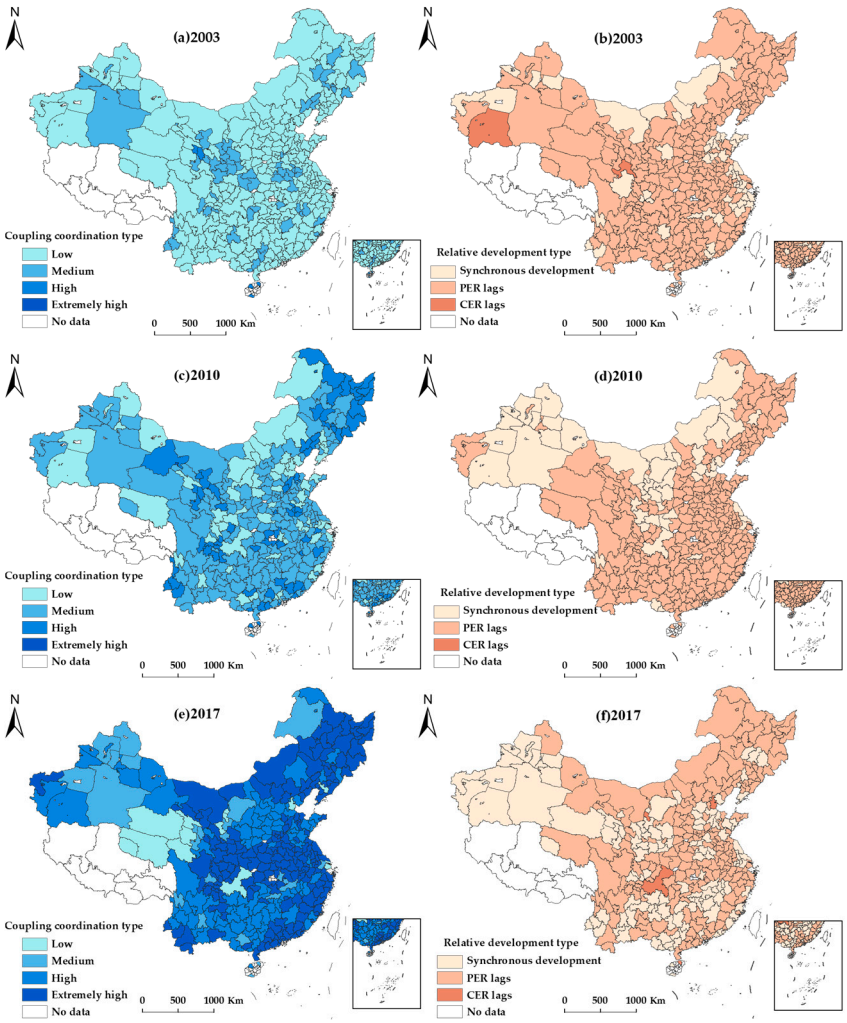

Figure 5. CCD of 329 cities in 2003, 2010, and 2017.

From the perspective of the relative development of CER and PER (Figure 5b,d,f), most cities were in the status of "PER lags" and "synchronous development" during the study period; "CER lags" were observed only in 2003 and 2017. Specifically, the cities in the status of "PER lags" accounted for 82.98%, 84.80%, and 60.18% of the total cities in 2003, 2010, and 2017, respectively, indicating a decreasing trend in the number of $PM_{2.5}$-emission-reduction lagged cities. By contrast, the ratio of cities in the status of "synchronous development" increased largely, increasing from 0.61% in 2003 to 38.60% in 2017. Only two (namely Gannan and Hotan) and four (namely Tianjin, Haikou, Chongqing, and Yinchuan) cities lagged in CER in 2003 and 2017, respectively.

3.2. Spatial Autocorrelation of CCD

The Global Moran's I indexes of the CCD of 329 cities in China from 2003 to 2017 were measured using the Geoda software. As reported in Table 2, the Global Moran's I value ranged from 0.0776 to 0.5016, with a mean value of 0.2779 ($p < 5\%$). The results show that there is a significant positive spatial autocorrelation among the CCDs of 329 cities in China.

Table 2. The Global Moran's I of CCD from 2003 to 2017.

Year	Moran's I	z-Value	*p*-Value
2003	0.2578	6.8480	0.005
2004	0.2927	8.6137	0.005
2005	0.2955	8.7381	0.005
2006	0.1971	6.8913	0.005
2007	0.2393	7.1758	0.005
2008	0.3198	9.5676	0.005
2009	0.2539	7.9959	0.005
2010	0.1612	4.6888	0.005
2011	0.5016	16.5871	0.005
2012	0.0776	2.4300	0.025
2013	0.4627	13.1608	0.005
2014	0.2274	6.9304	0.005
2015	0.3512	11.6491	0.005
2016	0.1380	4.2518	0.005
2017	0.3933	12.3570	0.005

To visually illustrate the overall spatial correlation of the CCD, we drew scatter plots of the CCD distributions in 329 cities for three representative years. As shown in Figure 6, the horizontal axis represents the standardized CCD, while the vertical axis denotes the CCD's spatial lag. It can be seen that 233 (71%), 210 (64%), and 248 (75%) cities were located in the first and third quadrants, i.e., "High–High" or "Low–Low" clustering zones, in 2003, 2010, and 2017, respectively, showing prominent positive spatial clustering characteristics. The Moran scatter plots further reveal the significant positive spatial autocorrelation of the CCDs among cities.

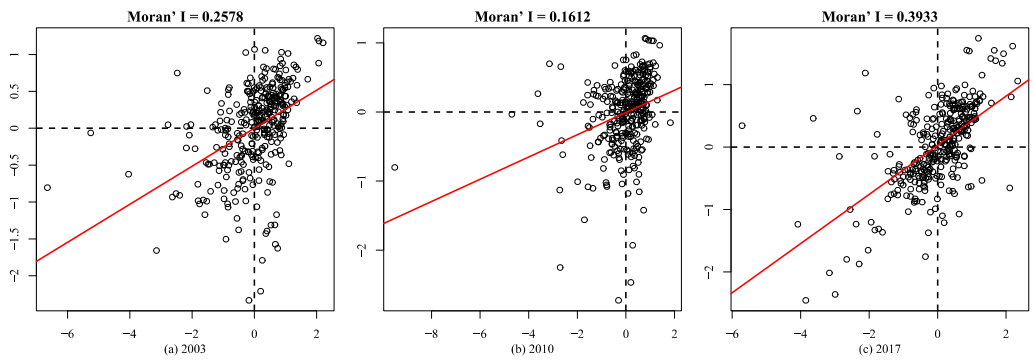

Figure 6. Moran scatter plots of the CCD in 2003, 2010, and 2017.

3.3. Evolutionary Characteristics of CCD

Figure 7 shows the dynamic trends of the CCD in China and its eight regions. From the perspective of distribution position and distribution shape, the kernel density curves for the CCD in China (Figure 7a) and its eight regions (Figure 7b–i) all displayed clear "right-shifted" trends from 2003 to 2017, implying increasing trends in the CCD; the height of the main peak of the national curve increased first and then decreased, while the width decreased first and then increased, indicating that the gaps for CCDs among cities narrowed first and then expanded. MYeR, MYR, and SW had similar changes in the shapes of the curves with the whole country, indicating that the intra-regional variations in the CCDs also decreased first and then increased. For NC, EC, and SC, the main peaks' heights all increased, while the widths decreased, indicating that the intra-regional variations of the CCD decreased. The opposite distribution trends occurred in NE and NW.

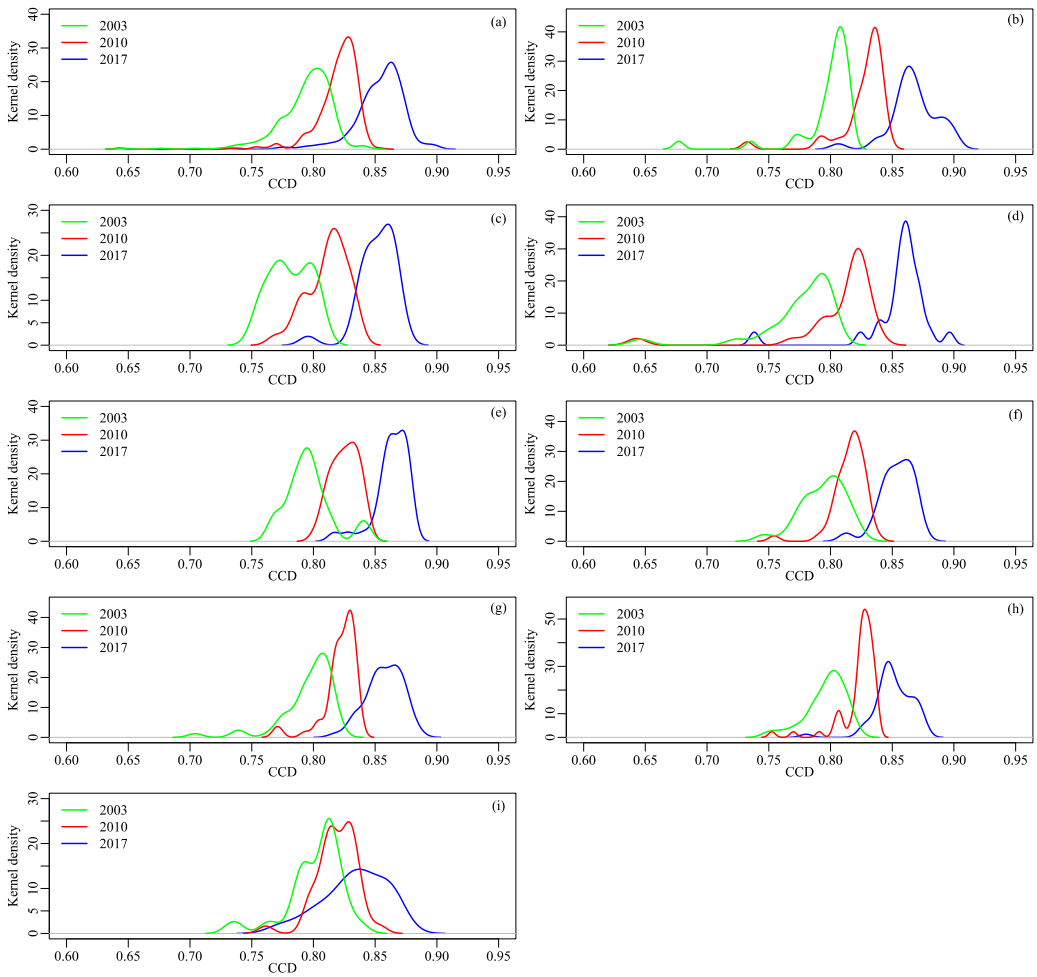

Figure 7. The dynamic evolutions of the CCD in China and its eight regions in 2003, 2010, and 2017: (**a**) China; (**b**) NE; (**c**) NC; (**d**) EC; (**e**) SC; (**f**) MYeR; (**g**) MYR; (**h**) SW and (**i**) NW.

For distribution ductility, obvious left-side tailings were observed in the curves of China and its eight regions, indicating that some cities' CCD values were obviously lower than those of other cities in the whole country or the regions. NE and EC had longer left-side tailings among the regions, especially in 2003. As illustrated in Figure 5, Anshan in NE and Shanghai in EC were cities with obviously lower CCDs than the others. MYR also had long left-side tailings in 2003, while the tailing became shorter in 2010 and 2017, indicating that the CCD values of the low-level coordinated cities in MYR were improved. In 2017, the tailing of NW had a thickening trend, implying an increase in the number of low-level coordinated cities.

Regarding polarization characteristics, China, EC, and MYeR showed obvious "single-peak" patterns during the period, indicating no polarization in these regions. SC, MYR, and SW experienced shifts from the patterns of "single-peak" to "double-peaks", indicating intensified polarization in these regions. In contrast, the polarization of NC and NW weakened, with the patterns changing from "double-peak" to "single-peak".

3.4. Reginal Differences in CCD

3.4.1. Intra-Regional Differences

Figure 8 reports the results of intra-regional Gini coefficients in the eight regions. EC had the highest mean value of the intra-regional Gini coefficient (0.018), followed by NW (0.0143) and NE (0.0135), suggesting the large variations in the CCD within these regions. The lowest mean value of the intra-regional Gini coefficient was observed in MYR (0.010), implying a small variation in the CCD in MYR. In terms of the changing trends of the intra-regional Gini coefficients, large fluctuations occurred in all the regions during the whole period. SC, MYeR, EC, MYR, and NC showed apparent fluctuating downward trends in intra-regional Gini coefficients, with total decreases of 34.50%, 29.42%, 27.75%, and 24.66% in the 15 years, respectively. These results indicate that the gaps in the CCD within the five regions narrowed. From 2003 to 2017, the intra-regional Gini coefficient increased from 0.0142 to 0.0172 in NW, showing an expanding gap in CCD within the region. For NE and SW, the intra-regional Gini coefficients fluctuated from 0.0069 to 0.0212 and from 0.0068 to 0.0160, respectively.

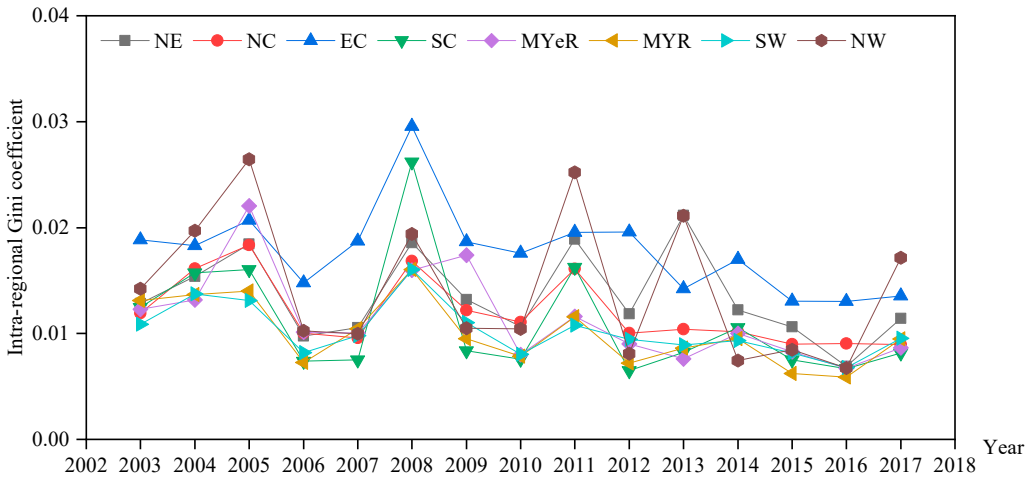

Figure 8. The intra-regional Gini coefficients from 2003 to 2017.

3.4.2. Inter-Regional Differences

Figure 9 reports the results of inter-regional Gini coefficients. EC-NW had the largest inter-regional Gini coefficient (0.0193), followed by NE-EC (0.0188), NE-NC (0.0182), and NC-NW (0.0178), indicating the large gap in CCD between coastal areas and northern inland areas. By contrast, MYR-SW had the lowest inter-regional Gini coefficient (0.0104). Concerning the changing trend, the inter-regional differences showed fluctuations before 2013. However, after 2013, most inter-regional Gini coefficients presented relatively stable decline trends. From 2003 to 2017, the largest drop was observed in NE-EC, with a total decrease of 0.0076. NE-EC exhibited a fluctuating increasing trend, reaching its peak (0.0274) in 2008, dropping to the lowest value (0.0109) in 2016, and finally rebounding to 0.0133 in 2017. EC-MYR and EC-MYeR also showed large declines in the inter-regional Gini coefficient, from 0.0194 to 0.0117 and from 0.0178 to 0.0116, respectively, with minor fluctuations. In contrast, SC-SW had the smallest fluctuation range in the inter-regional Gini coefficient (0.0071–0.0240). From 2003 to 2017, the inter-regional Gini coefficient of SC-SW decreased by only 0.09%.

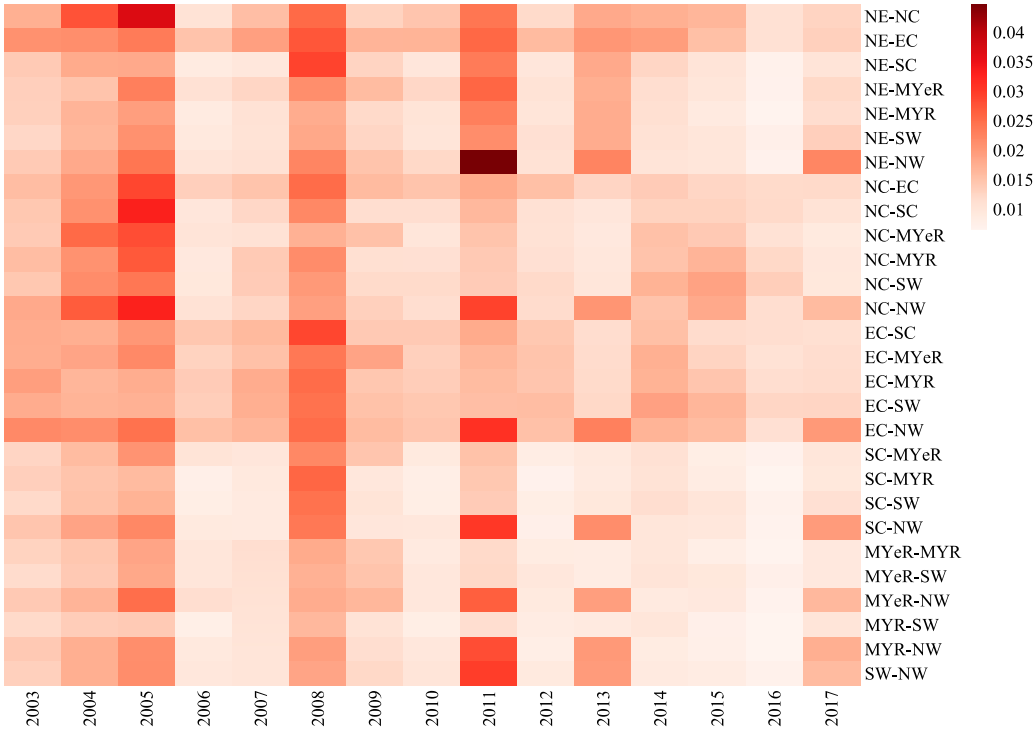

Figure 9. The inter-regional Gini coefficients from 2003 to 2017.

3.4.3. Sources of the Overall Difference

Figure 10 reports the decomposition results of the overall difference in CCD. The 15-year average contribution followed the order hypervariable density (0.0066) > inter-regional differences (0.0055) > intra-regional differences (0.0016). Similarly, the 15-year average contribution rate of hypervariable density was the largest (48.81%), followed by inter-regional differences (39.60%) and intra-regional differences (11.58%). The hypervariable density apparently accounted for the most significant difference in CCD overall. In contrast, the intra-regional differences had the smallest effect on the overall difference in CCD. From the perspective of the changing trends, the contribution rate of the hypervariable density showed an overall downward trend. It decreased from 57.47% in 2003 to 42.36% in 2017, with a decrease of 26.30%, suggesting a weakening effect of the hypervariable density on the overall difference. The contribution rate of the inter-regional differences showed a fluctuating upward trend. It increased from 30.43% in 2003 to 46.11% in 2017, indicating an intensifying effect of the inter-regional differences on the overall difference. Unlike hypervariable density and inter-regional differences, intra-regional differences only showed slight fluctuations, fluctuating around 11%.

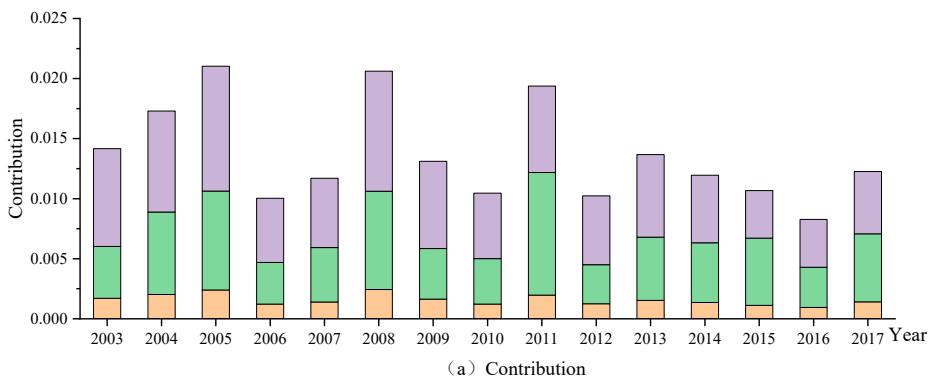

Figure 10. *Cont.*

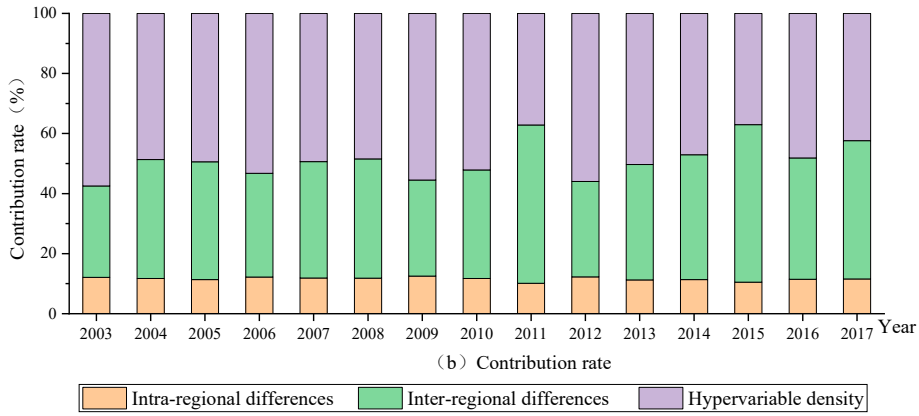

Figure 10. The sources of the overall difference in CCD during 2003–2017.

4. Discussion

4.1. Explanation for the Spatiotemporal Characteristics of CCD

Overall, the national average CCD showed an upward trend, indicating an improvement in the level of synergistic emission reduction of CO_2 and $PM_{2.5}$ in China. Our result is consistent with Tang et al.'s [31]. In recent years, China has implemented a series of measures to reduce CO_2 and $PM_{2.5}$ emissions, including eliminating outdated capacity, promoting clean energy, phasing out small coal-fired boilers, enforcing total coal consumption control, and retiring yellow labels and old vehicles. Specifically, since 2013, China has eliminated about 424 GW small coal-fired boilers, reducing inefficient coal consumption and thereby resulting in the synergistic benefits of CO_2 and $PM_{2.5}$ emissions' reduction [28]. In addition, due to non-compliance with national emission standards, approximately 26 million yellow labels and old vehicles were eliminated from 2003 to 2020 [28]. The package of policies and measures contributes most to the CO_2 and $PM_{2.5}$ emissions' reductions.

Among the eight regions, NE had the highest coupled coordinated level. On the one hand, NE has been plagued by economic recession and population loss for a long time, resulting in low total energy consumption and low emissions of CO_2 and $PM_{2.5}$. On the other hand, from 2006 to 2010, NE accelerated structural transformation and the development of a circular economy of resource-exhausted cities, improving energy efficiency and reducing CO_2 and $PM_{2.5}$ emissions. SC and EC also performed well in CCD, benefiting from their relatively reasonable industrial structure and high economic development level. Similar results were obtained from a previous study. Yi et al. [21] found that of the 11 provinces that achieved synergy between CO_2 emission reduction and pollution control in 2018, 5 are located in SC or EC. In the two regions, the proportion of service and high-tech industries is high; as a result, the energy consumption and emissions of CO_2 and $PM_{2.5}$ are relatively low. In addition, a high economic development level can enable the regions to invest more money in emission reductions. By contrast, NW had the lowest CCD, which agrees with Nie et al. [32]. They measured the synergy between carbon reduction and pollution control, finding that Xinjiang, Inner Mongolia, and Ningxia had the lowest CCD values in 2009. With rich coal and iron resources, the region's petroleum extraction and processing industries are densely distributed, leading to great CO_2 and $PM_{2.5}$ emissions. Moreover, because of an underdeveloped economy and low energy efficiency, NW had a high emission intensity and emission growth rate, which also lowered the synergy level of CO_2 and $PM_{2.5}$ emissions' reduction.

On the urban scale, the CCD of Shanghai was the lowest in 2003, 2010, and 2017. Though Shanghai performed well regarding emission intensity and the growth rate of emissions, its performance on the total CO_2 and $PM_{2.5}$ emissions was poor. In 2003, 2010, and 2017, the emissions of CO_2 were 139.42 Mt, 230.71 Mt, and 192.50 Mt, respectively, which were about 10, 8, and 6 times the national average level, respectively; and the emissions of $PM_{2.5}$ were 238,511 t, 575,583 t, and 515,521 t, respectively, which were 8, 15, and 16 times the national average level. The large CO_2 and $PM_{2.5}$ emissions led to the low

CCD level in Shanghai. Additionally, with regard to the relative development type, "$PM_{2.5}$ emission reduction lag" is the primary lagged type. China has been concerned about CO_2 emission reduction for a long time, while focusing on $PM_{2.5}$ pollution control only since 2013. Thus, for many cities, the governance of the $PM_{2.5}$ emissions lagged behind that of the CO_2 emissions.

4.2. Explanation for the Regional Differences in CCD

Regarding the intra-regional differences, EC had the highest inter-regional Gini coefficient. This may be attributed to the large variation in energy consumption within this region. For instance, due to the large scale of their population and economy, cities such as Suzhou and Shanghai in EC consumed 6315 and 5977 million tons of standard coal, respectively. However, many other cities, such as Zhoushan, Quzhou, and Lishui, consumed much lower energy than Suzhou and Shanghai, with values of 844, 921, and 929 million tons of standard coal, respectively. In terms of the inter-regional differences, the difference between EC and NW was the largest, while that between MYR and SW was the smallest. Compared with NW, EC had more advantages in technological innovation, energy structure, industrial structure, and environmental regulation intensity, and therefore the gap in the CCD values between the two regions is relatively large. In contrast, MYR and SW had great similarities in the abovementioned aspects. Furthermore, the hypervariable density played the most dominant role in the difference in CCD, followed by the inter-regional differences. The hypervariable density reflects the contribution of the cross-overlapping of samples to the overall difference [48]. Cross-overlapping refers to the phenomenon of some cities with extremely low CCD values located in the high-CCD-level regions or some cities with extremely high CCD values located in the low-CCD-level regions, such as Shanghai in EC and Anshan in NE. The high hypervariable density indicates a high number of cities involved in overlapping. Thus, to achieve the synergy between CO_2 and $PM_{2.5}$ emissions' reductions, the cross-overlapping problem among the eight regions should not be overlooked.

5. Conclusions and Policy Implications

5.1. Conclusions

This study focused on the synergy between CO_2 and $PM_{2.5}$ emissions' reductions in China from 2003 to 2017. We first calculated the CCD of CO_2 and $PM_{2.5}$ emissions' reductions in China's 329 cities and analyzed the spatiotemporal characteristics of the CCD on three spatial scales (i.e., national, regional, and urban scales). Then, we explored the spatial autocorrelation and evolutionary characteristics of the CCD. Finally, regional differences in CCD were examined. Key findings and principal conclusions are as follows:

- The synergy between CER and PER showed overall upward trends on three scales. On the national scale, the proportions of high-level and extremely high level coordinated cities increased largely, from 1.52% and 0 in 2003 to 31.31% and 58.05% in 2017, respectively. On the regional scale, NE, SC, and EC showed the best performance in CCD, while NW performed worst in CCD. On the urban scale, Shanghai had the lowest CCD values. In addition, from the perspective of the relative development of CER and PER, most cities were in the status of "PER lags" or "synchronous development" during the study period. The ratio of cities in the "synchronous development" status increased from 0.61% in 2003 to 38.60% in 2017.
- The CCD showed an obvious positive spatial autocorrelation. The Global Moran's I value ranged from 0.0776 to 0.5016, with a mean value of 0.2779. In Moran scatter plots, the cities in the "High–High" or "Low–Low" clustering zones accounted for 71%, 64%, and 75% of all the cities in 2003, 2010, and 2017, respectively, indicating strong clustering characteristics.
- The kernel density curves of CCD in China and the eight regions showed clear "right-shifted" trends and a left-side tailing phenomenon. In particular, due to the extremely lower CCD in individual cities, such as Anshan and Shanghai, NE and EC presented

very long left-side tailings. Moreover, the polarization of CCD in SC, MYR, and SW showed intensified trends, while that of NC and NW gradually weakened.

- As for the regional differences, EC showed the largest intra-regional difference, and the difference showed a fluctuating downward trend. The inter-regional difference between EC and NW was the largest, while that between MYR and SW was the smallest. The hypervariable density contributed most to the overall difference, followed by inter-regional and intra-regional differences, indicating that the cross-overlapping problem among the regions should not be overlooked.

The study still has some limitations. First, due to data limitations, the research period only spanned from 2003 to 2017. Since December 2019, the coronavirus pandemic has spread across China, and many anthropogenic activities have been restricted in the country, including transportation, industrial production, and construction. This may lead to reductions in both CO_2 and $PM_{2.5}$ emissions. The evaluation of the synergistic emission reduction level after 2017 may provide more information for policymakers. Thus, the period is expected to extend when data are available. Second, we compared the synergy level of CER and PER in only eight regions in China, which were divided according to the commonly used division criteria. Future work should focus on the synergy in China's key strategic regions and city clusters. Third, the reasons for the spatial and temporal differences in the synergy in China were analyzed primarily based on comparative inference. Therefore, the influencing factors of the synergy should be explored in detail in a future study.

5.2. Policy Implications

Based on the above conclusions, the following policy implications are presented.

Firstly, a top-level design is required for formulating policies. CO_2 and $PM_{2.5}$ emissions' reductions have a common target, and a high synergy is challenging to achieve with the separate CO_2- or $PM_{2.5}$-emission-reduction policies. Hence, the policies for synergistic emission reduction should focus on restructuring energy, improving energy efficiency, upgrading industrial structure, and the synergistic control of multi-pollutants.

Secondly, it is essential to enhance the role of technological innovation in the synergistic governance of CO_2 and $PM_{2.5}$ emissions. At present, the synergy degree of CO_2 and $PM_{2.5}$ emissions' reduction is limited by the technological level in some undeveloped cities in China. Thus, the investment in technological innovation in the synergistic governance of CO_2 and $PM_{2.5}$ should be increased. In addition, the new technologies which have achieved significant emission-reduction effects in some high-tech cities should be introduced to other cities.

Finally, it is vital to strengthen cooperation among cities and even among regions. Because both CO_2 and $PM_{2.5}$ emissions showed spatial agglomeration characteristics, stronger industrial and technological cooperation between regions is crucial for reducing emissions. In particular, cooperation regarding industrial transfer, energy consumption reduction, clean energy utilization, and energy-saving technologies should be emphasized.

Author Contributions: Conceptualization, S.W., S.Z. and L.C.; methodology, S.W. and L.C.; software, S.W.; validation, S.W. and L.C.; formal analysis, S.W. and L.C.; investigation, S.W. and L.C.; data curation, S.W. and L.C.; writing—original draft preparation, S.W.; writing—review and editing, S.W., S.Z. and L.C.; visualization, S.W.; supervision, S.Z. All authors have read and agreed to the published version of the manuscript.

Funding: This work was supported by the National Natural Science Foundation of China, grant numbers 11926354 and 72073038; Technology Planning Project of Shaoguan, grant numbers 210726224533614 and 210726214533591; Philosophy and Social Science Program of Shaoguan, grant number J2020008; Social Science Program of Shaoguan University, grant number SY2020SK02; Talent Project of Shaoguan University, grant number 9900064502; Natural Science Foundation of Guangdong Province, grant numbers 2022A1515011358 and 2023A1515010825.

Institutional Review Board Statement: Not applicable.

Informed Consent Statement: Not applicable.

Data Availability Statement: CO_2 emission data available online at https://www.ceads.net.cn/ (accessed on 10 May 2023); $PM_{2.5}$ emission data available online at https://edgar.jrc.ec.europa.eu/ (accessed on 12 May 2023); and GDP data can be collected from the China City Statistical Yearbook (https://data.cnki.net/yearBook/single?id=N2022040095, accessed on 15 May 2023).

Conflicts of Interest: The authors declare no conflict of interest.

Appendix A

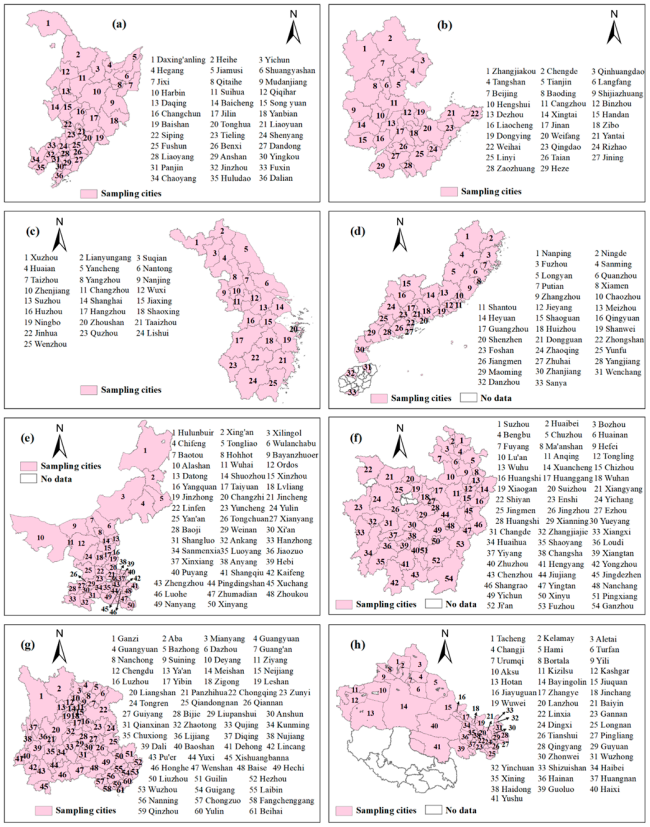

Figure A1. The full names of the cities in the eight regions: (**a**) NE, (**b**) NC, (**c**) EC, (**d**) SC, (**e**) MYeR, (**f**) MYR, (**g**) SW, and (**h**) NW.

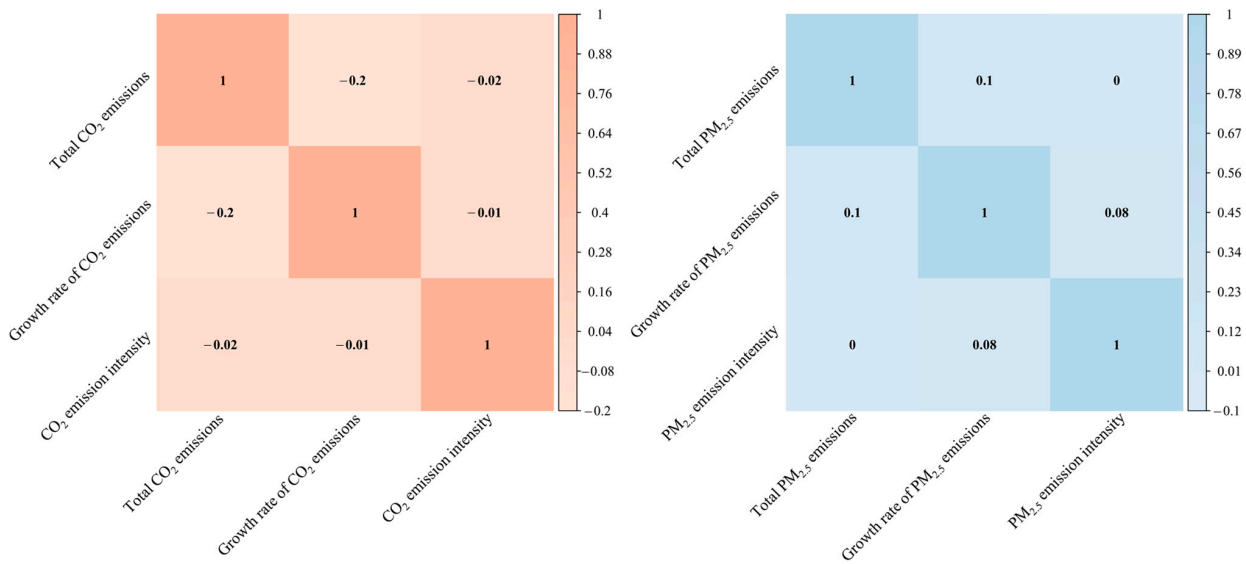

Figure A2. Results of the Peason correlation analysis.

References

1. Elahi, E.; Khalid, Z.; Tauni, M.Z.; Zhang, H.X.; Xing, L.R. Extreme weather events risk to crop-production and the adaptation of innovative management strategies to mitigate the risk: A retrospective survey of rural Punjab, Pakistan. *Technovation* **2022**, *117*, 102255. [CrossRef]
2. Elahi, E.; Khalid, Z.; Zhang, Z.X. Understanding farmers' intention and willingness to install renewable energy technology: A solution to reduce the environmental emissions of agriculture. *Appl. Energy* **2022**, *309*, 118459. [CrossRef]
3. Abbas, A.; Waseem, M.; Ahmad, R.; Khan, K.A.; Zhao, C.Y.; Zhu, J.T. Sensitivity analysis of greenhouse gas emissions at farm level: Case study of grain and cash crops. *Environ. Sci. Pollut. Res.* **2022**, *29*, 82559–82573. [CrossRef]
4. Abbas, A.; Zhao, C.Y.; Waseem, M.; Khan, K.A.; Ahmad, R. Analysis of Energy Input-Output of Farms and Assessment of Greenhouse Gas Emissions: A Case Study of Cotton Growers. *Front. Environ. Sci.-Switz.* **2022**, *9*, 826838. [CrossRef]
5. Guan, Y.; Xiao, Y.; Rong, B.; Lu, W.T.; Zhang, N.N.; Qin, C.B. Assessing the synergy between CO_2 emission and ambient $PM_{2.5}$ pollution in Chinese cities: An integrated study based on economic impact and synergy index. *Environ. Impact Asses* **2023**, *99*, 106989. [CrossRef]
6. Yu, Y.J.; Dai, C.; Wei, Y.G.; Ren, H.M.; Zhou, J.W. Air pollution prevention and control action plan substantially reduced $PM_{2.5}$ concentration in China. *Energy Econ.* **2022**, *113*, 106206. [CrossRef]
7. Li, S.; Wang, S.; Wu, Q.; Zhang, Y.; Ouyang, D.; Zheng, H.; Han, L.; Qiu, X.; Wen, Y.; Liu, M.; et al. Emission trends of air pollutants and CO_2 in China from 2005 to 2021. *Earth Syst. Sci. Data* **2023**, *15*, 2279–2294. [CrossRef]
8. Harrould-Kolieb, E.R. Framing ocean acidification to mobilise action under multilateral environmental agreements. *Environ. Sci. Policy* **2020**, *104*, 129–135. [CrossRef]
9. Gregg, J.S.; Andres, R.J.; Marland, G. China: Emissions pattern of the world leader in CO_2 emissions from fossil fuel consumption and cement production. *Geophys. Res. Lett.* **2008**, *35*, L08806. [CrossRef]
10. Wu, J.Q.; Chen, Y.; Yu, L.; Li, J.K. Coupling effects of consumption side renewable portfolio standards and carbon emission trading scheme on China's power sector: A system dynamic analysis. *J. Clean. Prod.* **2022**, *380*, 134931. [CrossRef]
11. Kelly, F.J.; Fussell, J.C. Air pollution and public health: Emerging hazards and improved understanding of risk. *Environ. Geochem. Health* **2015**, *37*, 631–649. [CrossRef]
12. Bala, G.P.; Rajnoveanu, R.M.; Tudorache, E.; Motisan, R.; Oancea, C. Air pollution exposure-the (in)visible risk factor for respiratory diseases. *Environ. Sci. Pollut. Res.* **2021**, *28*, 19615–19628. [CrossRef]
13. Orellano, P.; Reynoso, J.; Quaranta, N.; Bardach, A.; Ciapponi, A. Short-term exposure to particulate matter (PM_{10} and $PM_{2.5}$), nitrogen dioxide (NO_2), and ozone (O_3) and all-cause and cause-specific mortality: Systematic review and meta-analysis. *Environ. Int.* **2020**, *142*, 105876. [CrossRef]
14. McDuffie, E.E.; Martin, R.V.; Spadaro, J.V.; Burnett, R.; Smith, S.J.; O'Rourke, P.; Hammer, M.S.; van Donkelaar, A.; Bindle, L.; Shah, V.; et al. Source sector and fuel contributions to ambient $PM_{2.5}$ and attributable mortality across multiple spatial scales. *Nat. Commun.* **2021**, *12*, 3594. [CrossRef] [PubMed]
15. Zhang, R.H.; Li, Q.; Zhang, R.N. Meteorological conditions for the persistent severe fog and haze event over eastern China in January 2013. *Sci. China Earth Sci.* **2014**, *57*, 26–35. [CrossRef]
16. Huang, R.J.; Zhang, Y.L.; Bozzetti, C.; Ho, K.F.; Cao, J.J.; Han, Y.M.; Daellenbach, K.R.; Slowik, J.G.; Platt, S.M.; Canonaco, F.; et al. High secondary aerosol contribution to particulate pollution during haze events in China. *Nature* **2014**, *514*, 218–222. [CrossRef]
17. Zhi, G.R.; Zhang, Y.Y.; Sun, J.Z.; Cheng, M.M.; Dang, H.Y.; Liu, S.J.; Yang, J.C.; Zhang, Y.Z.; Xue, Z.G.; Li, S.Y.; et al. Village energy survey reveals missing rural raw coal in northern China: Significance in science and policy. *Environ. Pollut.* **2017**, *223*, 705–712. [CrossRef]
18. Jiang, L.; Bai, L. Spatio-temporal characteristics of urban air pollutions and their causal relationships: Evidence from Beijing and its neighboring cities. *Sci. Rep.* **2018**, *8*, 1279. [CrossRef] [PubMed]
19. Huang, J.; Pan, X.C.; Guo, X.B.; Li, G.X. Health impact of China's Air Pollution Prevention and Control Action Plan: An analysis of national air quality monitoring and mortality data. *Lancet Planet. Health* **2018**, *2*, E313–E323. [CrossRef] [PubMed]
20. Jiang, X.; Li, G.L.; Fu, W. Government environmental governance, structural adjustment and air quality: A quasi-natural experiment based on the Three-year Action Plan to Win the Blue Sky Defense War. *J. Environ. Manag.* **2021**, *277*, 111470. [CrossRef]
21. Yi, H.R.; Zhao, L.J.; Qian, Y.; Zhou, L.X.; Yang, P.L. How to achieve synergy between carbon dioxide mitigation and air pollution control? Evidence from China. *Sustain. Cities Soc.* **2022**, *78*, 103609. [CrossRef]
22. Yu, Y.; Jin, Z.X.; Li, J.Z.; Jia, L. Low-carbon development path research on China's power industry based on synergistic emission reduction between CO_2 and air pollutants. *J. Clean. Prod.* **2020**, *275*, 123097. [CrossRef]
23. Yang, H.C.; Gan, T.; Liang, W.; Liao, X.C. Can policies aimed at reducing carbon dioxide emissions help mitigate haze pollution? An empirical analysis of the emissions trading system. *Environ. Dev. Sustain.* **2022**, *24*, 1959–1980. [CrossRef]
24. Yang, X.; Yang, X.; Zhu, J.; Jiang, P.; Lin, H.; Cai, Z.; Huang, H. Achieving co-benefits by implementing the low-carbon city pilot policy in China: Effectiveness and efficiency. *Environ. Technol. Innov.* **2023**, *30*, 103137. [CrossRef]
25. Chen, S.Y.; Wang, C. Health benefits from the reduction of $PM_{2.5}$ concentrations under carbon tax and emission trading scheme: A case study in China. *Environ. Sci. Pollut. Res.* **2022**, *30*, 36631–36645. [CrossRef]
26. Dong, F.; Yu, B.L.; Pan, Y.L. Examining the synergistic effect of CO_2 emissions on $PM_{2.5}$ emissions reduction: Evidence from China. *J. Clean. Prod.* **2019**, *223*, 759–771. [CrossRef]

27. Jia, W.L.; Li, L.; Lei, Y.L.; Wu, S.M. Synergistic effect of CO_2 and $PM_{2.5}$ emissions from coal consumption and the impacts on health effects. *J. Environ. Manag.* **2023**, *325*, 116535. [CrossRef]
28. Shi, Q.; Zheng, B.; Zheng, Y.; Tong, D.; Liu, Y.; Ma, H.; Hong, C.; Geng, G.; Guan, D.; He, K.; et al. Co-benefits of CO_2 emission reduction from China's clean air actions between 2013–2020. *Nat. Commun.* **2022**, *13*, 5061. [CrossRef]
29. Yang, H.Z.; Liu, J.F.; Jiang, K.J.; Meng, J.; Guan, D.B.; Xu, Y.; Tao, S. Multi-objective analysis of the co-mitigation of CO_2 and $PM_{2.5}$ pollution by China's iron and steel industry. *J. Clean. Prod.* **2018**, *185*, 331–341. [CrossRef]
30. Xing, Y.; Mao, X.; Feng, X.; Gao, Y.; He, F.; Yu, H.; Zhao, M. An effectiveness evaluation of co-controlling local air pollutants and GHGs by implementing Blue Sky Defense Action at city level—A case study of Tangshan city. *Chin. J. Environ. Manag.* **2020**, *12*, 20–28. [CrossRef]
31. Tang, X.; Zhang, Y.; Cao, L.; Zhang, J.; Chen, X. Spatio-Temporal Characteristics and Influencing Mechanism of Synergistic Effect of Pollution and Carbon Emission Reduction in China. *Res. Environ. Sci.* **2022**, *35*, 2252–2263. [CrossRef]
32. Nie, C.F.; Lee, C.-C. Synergy of pollution control and carbon reduction in China: Spatial—Temporal characteristics, regional differences, and convergence. *Environ. Impact Assess. Rev.* **2023**, *101*, 107110. [CrossRef]
33. Li, Y.; Cui, Y.; Cai, B.; Guo, J.; Cheng, T.; Zheng, F. Spatial characteristics of CO_2 emissions and $PM_{2.5}$ concentrations in China based on gridded data. *Appl. Energy* **2020**, *266*, 114852. [CrossRef]
34. Yan, D.; Ren, X.H.; Kong, Y.; Ye, B.; Liao, Z.Y. The heterogeneous effects of socioeconomic determinants on $PM_{2.5}$ concentrations using a two-step panel quantile regression. *Appl. Energy* **2020**, *272*, 115246. [CrossRef]
35. Chen, J.Y.; Luo, W.J.; Ren, X.H.; Liu, T.Q. The local-neighborhood effects of low-carbon city pilots program on $PM_{2.5}$ in China: A spatial difference-in-differences analysis. *Sci. Total Environ.* **2023**, *857*, 159511. [CrossRef]
36. Liu, Z.; Wang, F.; Tang, Z.Y.; Tang, J.T. Predictions and driving factors of production-based CO_2 emissions in Beijing, China. *Sustain. Cities Soc.* **2020**, *53*, 101909. [CrossRef]
37. Zhang, B.L.; Yin, S.S.; Lu, X.; Wang, S.F.; Xu, Y.F. Development of city-scale air pollutants and greenhouse gases emission inventory and mitigation strategies assessment: A case in Zhengzhou, Central China. *Urban Clim.* **2023**, *48*, 101419. [CrossRef]
38. Li, L.; Mi, Y.F.; Lei, Y.L.; Wu, S.M.; Li, L.; Hua, E.S.; Yang, J.J. The spatial differences of the synergy between CO_2 and air pollutant emissions in China's 296 cities. *Sci. Total Environ.* **2022**, *846*, 157323. [CrossRef]
39. Lai, Z.; Ge, D.; Xia, H.; Yue, Y.; Wang, Z. Coupling coordination between environment, economy and tourism: A case study of China. *PLoS ONE* **2020**, *15*, e0228426. [CrossRef] [PubMed]
40. Liu, F.; Tang, L.; Liao, K.; Ruan, L.; Liu, P. Spatial distribution and regional difference of carbon emissions efficiency of industrial energy in China. *Sci. Rep.* **2021**, *11*, 19419. [CrossRef] [PubMed]
41. Oreggioni, G.D.; Mahiques, O.; Monforti-Ferrario, F.; Schaaf, E.; Muntean, M.; Guizzardi, D.; Vignati, E.; Crippa, M. The impacts of technological changes and regulatory frameworks on global air pollutant emissions from the energy industry and road transport. *Energy Policy* **2022**, *168*, 113021. [CrossRef]
42. Ji, J.; Liu, H.; Yin, X. Evaluation and regional differences analysis of the marine industry development level: The Case of China. *Mar. Policy* **2023**, *148*, 105445. [CrossRef]
43. Xia, D.; Zhang, L. Coupling coordination degree between coal production reduction and CO_2 emission reduction in coal industry. *Energy* **2022**, *258*, 124902. [CrossRef]
44. Wen, H.; Liang, W.; Lee, C.-C. China's progress toward sustainable development in pursuit of carbon neutrality: Regional differences and dynamic evolution. *Environ. Impact Assess. Rev.* **2023**, *98*, 106959. [CrossRef]
45. Tomal, M. Evaluation of coupling coordination degree and convergence behaviour of local development: A spatiotemporal analysis of all Polish municipalities over the period 2003–2019. *Sustain. Cities Soc.* **2021**, *71*, 102992. [CrossRef]
46. Shen, L.; Yang, Y.; Bao, H.; Du, X.; He, H. Residents' perceptions on the urban resources environment in Chinese large cities. *Environ. Impact Assess. Rev.* **2023**, *100*, 107080. [CrossRef]
47. Ma, T.; Liu, Y.; Yang, M. Spatial-Temporal Heterogeneity for Commercial Building Carbon Emissions in China: Based the Dagum Gini Coefficient. *Sustainability* **2022**, *14*, 5243. [CrossRef]
48. Chen, Z.; Zhang, Z.; Feng, T.; Liu, D. What drives the temporal dynamics and spatial differences of urban and rural household emissions in China? *Energy Econ.* **2023**, *125*, 106849. [CrossRef]